Rate equation of steam-methane reforming reaction on Ni-YSZ cermet considering its porous microstructure

S Sugihara[1,2], Y Kawamura[1] and H Iwai[1]

[1]Department of Aeronautics and Astronautics, Kyoto University, Kyoto, 615-8540, Japan

[2]Corporate R&D Div.2, DENSO CORPORATION, Aichi, 448-8661, Japan

E-mail: shinichi_sugihara@denso.co.jp

Abstract. The steam-methane reforming reaction on a Ni-YSZ (yttria-stabilized zirconia) cermet was experimentally investigated in the temperature range of 650 to 750℃. We examined the effects of the partial pressures of methane and steam in the supply gas on the reaction rate. The porous microstructure of the Ni-YSZ cermet was quantified using an FIB-SEM technique. A power-law-type rate equation was obtained on the basis of the unit surface area of the Ni-pore contact surface in the cermet. The kinetics indicated a strong positive dependence on the methane partial pressure and a negative dependence on the steam partial pressure, in good agreement with the literature. The obtained rate equation successfully predicted the reaction characteristics of Ni-YSZ cermets having different microstructures.

1. Introduction

Solid oxide fuel cell (SOFC) systems are recognized as a promising technology owing to their high generation efficiency of more than 50%. Fuel flexibility is also an attractive feature of the systems. In addition, internal reforming can also be applied to SOFCs because the Ni contained in the anode is a good catalyst for the steam reforming of hydrocarbon fuels. Internal reforming has two advantages; one is cost reduction by reducing the amount of expensive catalyst in the pre-reformer, and the other is improved efficiency by reducing the power required for air pumping to cool the cells because the reforming reaction is strongly endothermic. For example, the overall reformation process of methane rapidly consumes approximately 60% of the heat generated in the cell under the conditions of 75% fuel utilization, a temperature of 700℃ and 55% DC efficiency [1]. In exchange for these advantages, a strong temperature gradient may occur on the cell surface that can cause cell fracture and gas seal leakage. Hence, control of the internal reforming reaction is critically important.

Investigations have been intensively conducted on steam-methane reforming on SOFC anodes. However, two issues remain. Firstly, although there are various kinetic expressions, they are generally inconsistent with each other. Lee *et al.* investigated the methane conversion rate on different crushed Ni/ZrO_2 cermets while varying the H_2O/CH_4 ratio and temperature in the ranges of 2.7 to 7.4 and 800 to 1000℃, respectively [2]. The results showed that the steam partial pressure had a strong effect on the methane conversion rate. On the other hand, Achenbach and Riensche investigated reaction parameters under a total pressure of 1.1 to 2.8 bar and from 700 to 930℃, and reported that there was no effect of the steam partial pressure [3]. Mogensen *et al.* reviewed earlier literature and grouped the kinetic expressions into three types; Langmuir Hinshelwood (LH) kinetics, first order (FO) reaction with respect to methane, and power law (PL) expressions with respect to the composing gases. A comparison of 11 kinetics based on both industrial steam-methane reforming catalysts and Ni-YSZ for SOFCs showed that they were inconsistent [4]. Secondly, rate equations for industrial catalysts are generally evaluated for a unit weight of Ni contained in the catalysts [2][3]. Unfortunately, this makes it difficult to apply these rate equations to actual SOFC development because the weight of Ni does not reflect the reaction surface area of an SOFC anode. Additional attempts have been made to interpret the weight as a surface area [5-7]. However, it is unclear whether a correlation can be universally applied to any anode regardless of its porous microstructure. On the other hand, a special technique using focused ion beam scanning electron microscopy (FIB-SEM) has been newly developed that enables the direct quantification of a porous microstructure [8].

Considering the above, in this study, the rate equation of steam-methane reforming based on the anode microstructure was investigated. We performed reforming experiments on a small sample of a Ni-YSZ anode, followed by the quantification of the microstructure of the sample using the FIB-SEM technique. A rate equation for a unit surface area of Ni in the anode is estimated and its applicability to other samples having different microstructures is examined.

2. Fundamentals

2.1. Basic principles

The reforming process of methane is described by the following two equations.

$$\mathrm{CH_4 + H_2O = 3H_2 + CO} \tag{1}$$

$$\mathrm{CO + H_2O = H_2 + CO_2} \tag{2}$$

The former is well known as the strongly endothermic steam reforming reaction, and the latter is the slightly exothermic water-gas shift reaction. The reaction rate in this study is actually considered to be that of steam-methane reforming because the water-gas shift reaction at high temperature is a fast process and reaches equilibrium instantaneously. As mentioned above, there are three expressions used to describe the reaction kinetics. With regard to the kinetic expression, the following PL expression containing the methane and steam partial pressures is adopted in this study to avoid complexity and a high calculation cost in practical use.

$$R_{smr} = k_{smr}\left(P_{\mathrm{CH_4}}\right)^a\left(P_{\mathrm{H_2O}}\right)^b \tag{3}$$

$$k_{smr} = A\exp(-E\,/\,\mathrm{R_0}T) \tag{4}$$

In equation (3), R_{smr} is the methane consumption rate per second and per unit exposed Ni area, k_{smr} is the reaction coefficient and $P_{\mathrm{CH_4}}$and $P_{\mathrm{H_2O}}$ are the partial pressures of methane and steam at the reaction site, respectively. In equation (4), A is the frequency factor and E is the activation energy of the reaction. The aim of this study is to reveal the unknown values of a, b, A and E in relation to the exposed area of Ni in the anode microstructure.

The microstructure of the sample is quantified by the FIB-SEM technique [8]. FIB-SEM produces a series of cross-sectional images, as shown in figure 1, which are then processed and calculations are performed to quantify microstructural properties, for example, area density of exposed Ni, the volume fractions of Ni and YSZ, and so forth.

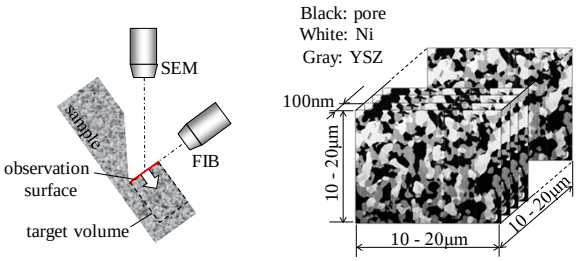

Figure 1. Schematic diagram of FIB-SEM setup.

The quantified area density of exposed Ni also enables us to express R_{smr} as follows.

$$R_{smr} = \Delta F_{\mathrm{CH_4}} \,/\, S_{Ni-pore} \tag{5}$$

Here, $\Delta F_{\mathrm{CH_4}}$ is the methane consumption rate and $S_{Ni-pore}$ is the total area of Ni facing the pores in the sample. $S_{Ni-pore}$ is obtained as follows.

$$S_{Ni-pore} = W_{sample} \,/\, \rho \cdot A_{Ni-pore} \tag{6}$$

W_{sample} is the weight of the sample and ρ is the sample density. $A_{Ni-pore}$ is the surface area of Ni facing the pores per unit volume of the sample obtained by the FIB-SEM technique. Note that equation (5) makes it very easy to calculate the methane consumption rate but it is only reliable when the temperature and gas compositions at the surface of Ni are nearly constant. To ensure them, the sample was fabricated as thin as possible to reduce mass transport delay and the methane conversion rate φ calculated by equation (7) was maintained as low as possible in this study. Here, X expresses the volume fraction of each gas at the outlet.

$$\varphi = (X_{\mathrm{CO}} + X_{\mathrm{CO_2}}) \,/\, (X_{\mathrm{CH_4}} + X_{\mathrm{CO}} + X_{\mathrm{CO_2}}) \tag{7}$$

Under this condition, equations (3) and (5) can be combined as follows.

$$k_{smr} = \left(P_{\mathrm{CH_4}}\right)^{-a}\left(P_{\mathrm{H_2O}}\right)^{-b} \cdot \Delta F_{\mathrm{CH_4}} \,/\, S_{Ni-pore} \tag{8}$$

In equation (8), the partial pressures of methane and steam are those before reaching sample. k_{smr} is assumed to be constant at a given temperature in this study. Assuming values of a and b, multiple values of k_{smr} can be obtained from experiments by varying $P_{\mathrm{CH_4}}$, $P_{\mathrm{H_2O}}$ and $\Delta F_{\mathrm{CH_4}}$. In this study, a and b are determined to minimize the value calculated by equation (9) in the range of $-1.0 \le a \le 2.0$ and $-2.0 \le b \le 1.0$.

$$\sigma^{ab} = \frac{1}{\overline{k_{smr}^{ab}}}\left\{\frac{1}{n}\sum_{l=1}^{n}\left(k_{smr,l}^{ab} - \overline{k_{smr}^{ab}}\right)^2\right\}^{1/2} \tag{9}$$

$$\overline{k_{smr}^{ab}} = \frac{1}{n}\sum_{l=1}^{n} k_{smr,l}^{ab} \tag{10}$$

The frequency factor A and activation energy E are also obtained by fitting equation (11) to experimental data.

$$\ln k_{smr} = \ln A - E \,/\, \mathrm{R_0}T \tag{11}$$

2.2. Fabrication of test sample

A large NiO-YSZ cermet sheet of thickness 0.1mm was fabricated and cut into approximately 10×10mm^2 squares for use in the following experiments.

2.3. Experimental setup

The experimental setup is composed of three sections as shown in figure 2.

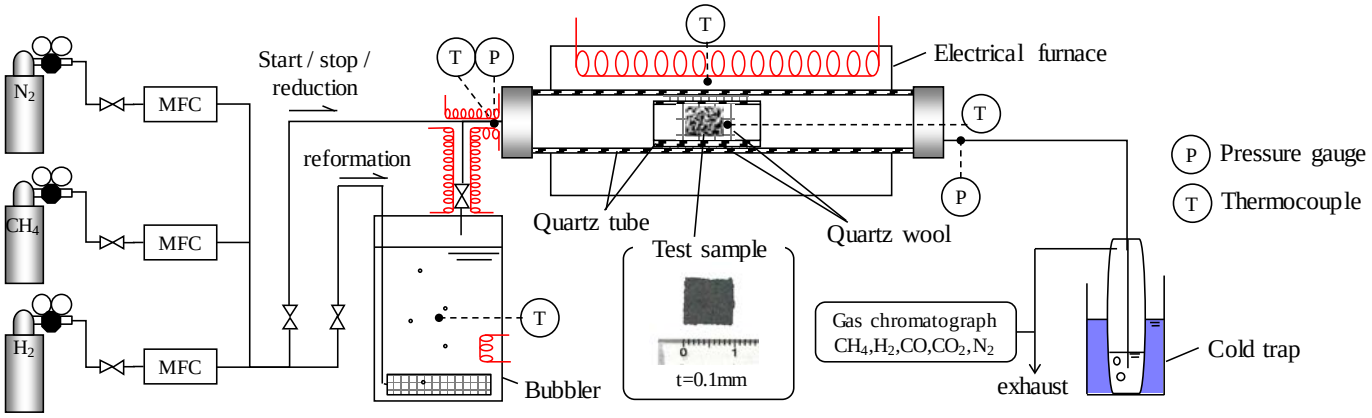

Figure 2. Experimental setup.

2.3.1. Gas supply. This section contains gas supply lines of nitrogen, methane, hydrogen and steam. All lines are connected by SUS316 1/4 inch pipes and swagelok joints. All gases can pass through a bubbler to remove steam. The relationship between the bubbler temperature and the removal rate of steam shows a good correspondence with the theoretical one. There is also a by-pass line only for the start-up, reduction and shut-down procedures. The lines connecting the bubbler outlet to the reactor inlet are heated to prevent condensation of steam.

2.3.2. Reaction. The sample is set parallel to the flow with quartz wool in a short 10mm-inner-diameter quartz tube to ensure the flow uniformity and the mass transport from both faces of the sample. The short tube is inserted into a long 20mm-inner-diameter tube so that it is at the center of the furnace. The ends of the outer tube are sealed completely by swagelok joints using Teflon ferrules. The pressure is measured at the inlet and outlet ends of the outer quartz tube, and the temperature is measured at the center point of the furnace and near the sample.

2.3.3. Analysis. After the reactor, the gases pass through a cold trap and are exhausted. After removing steam at the cold trap, the gasses are removed immediately after the cold trap and are analyzed by a gas chromatograph, where volume fractions of CH_4, H_2, CO, CO_2 and N_2 gases are detected.

2.4. Preliminary test

The gas seal of all the lines were checked at 10kPa inner pressure. The reduction procedure was conducted for 1h using pure hydrogen at 800℃.

It is well known that the carbon formation and catalytic degradation are two major issues in steam-methane reformation [9,10,5]. In this study, the steam-carbon ratio (S/C) was always maintained at more than 1.8 to avoid carbon formation [9]. With regard to catalytic degradation, a durability test has been conducted at temperatures of 650, 700 and 750℃ under a constant feed gas. The time trends of the volume fractions of CO and CO_2 in the exhaust gas are shown in figure 3. The degradation of the methane conversion rate given by equation (7) can be calculated from these results and equations (1) and (2) as shown in table 1. The degradation of the methane conversion rate in the following experiments appears to be less than 0.89 % because each experiments finishes within 10h.

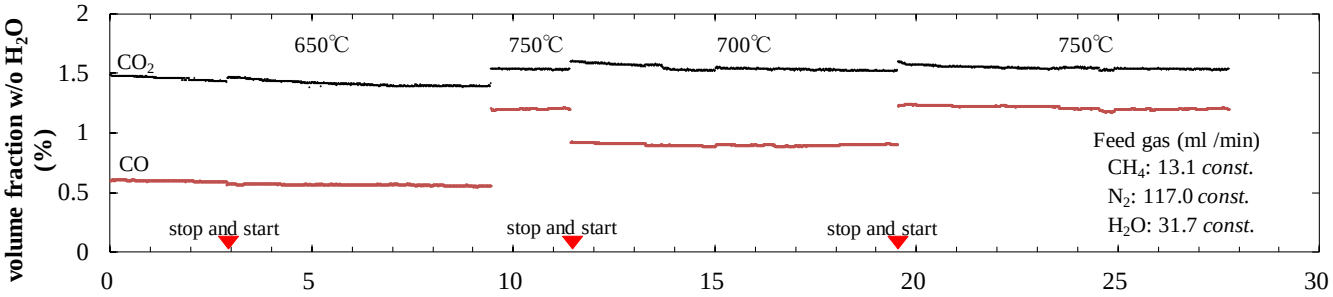

Figure 3. Time trend of volume fractions of CO and CO_2 in the exhaust gas under a constant gas feed.

Table 1. Degradation rate of methane conversion rate.

temperature	℃	650	700	750
degradation rate	% / h	-0.085	-0.089	-0.074

3. Results and Discussion

3.1. Microstructure of test sample

The properties of the microstructure quantified by the FIB-SEM technique are shown in table 2, as well as some of the corresponding fabrication data. These quantified data appear to be valid because the Ni/YSZ volume fraction ratio shows a good correspondence with the fabrication data. A 2D image figure and reconstructed 3D model are shown in figure 4. The white and gray parts represent Ni and YSZ, respectively.

Table 2. Quantified microstructural parameters of sample.

	volume fraction				$S_{Ni\text{-}pore}$
	Ni	YSZ	Pore	Ni / YSZ ratio	(m^2/m^3)
quantified data	0.065	0.490	0.444	0.133	55700
fabrication data	-	-	-	0.137 [a]	-

[a] Estimated from NiO/YSZ ratio

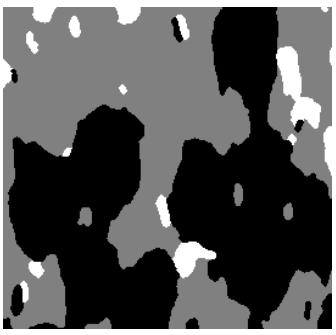

White: Ni
Gray: YSZ
Black: pore

(a) Typical cross-section.

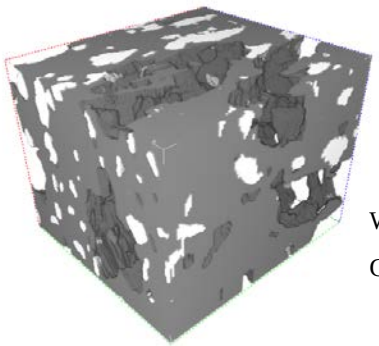

White: Ni
Gray: YSZ

(b) 3D reconstructed microstructure.

Figure 4. Configurations of test sample.

3.2. Reaction and analysis

The experimental conditions are shown in detail in table 3. Condition Nos.1 to 11 are set to investigate the dependence of the conversion rate on the methane and steam partial pressures. Nos.12 to 15 are set to investigate the temperature dependence. The results of tests Nos.1 to 11 are converted into R_{smr} values and are shown in figures 5 and 6.

Table 3. Experimental conditions.

No.	CH_4(ml/min)	H_2O(ml/min)	N_2(ml/min)	temperature (℃)	S/C
1	4.0	44.3	96.0	700	11.07
2	8.0	18.3	92.0	700	2.29
3	8.0	24.4	92.0	700	3.05
4	8.0	27.4	92.0	700	3.42
5	8.0	32.7	92.0	700	4.08
6	8.0	36.8	92.0	700	4.60
7	8.0	44.3	92.0	700	5.53
8	12.0	44.3	88.0	700	3.69
9	16.0	44.3	84.0	700	2.77
10	20.0	44.3	80.0	700	2.21
11	24.0	44.3	76.0	700	1.84
12	8.0	44.3	92.0	750	5.53
13	8.0	44.3	92.0	725	5.53
14	8.0	44.3	92.0	675	5.53
15	8.0	44.3	92.0	650	5.53

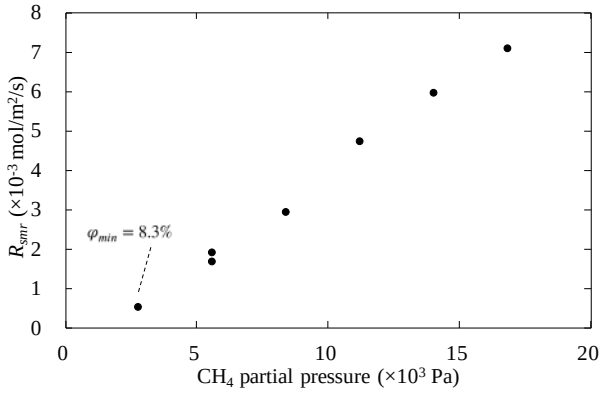

Figure 5. Dependence on methane partial pressure (condition Nos. 1,7,8,9,10,11).

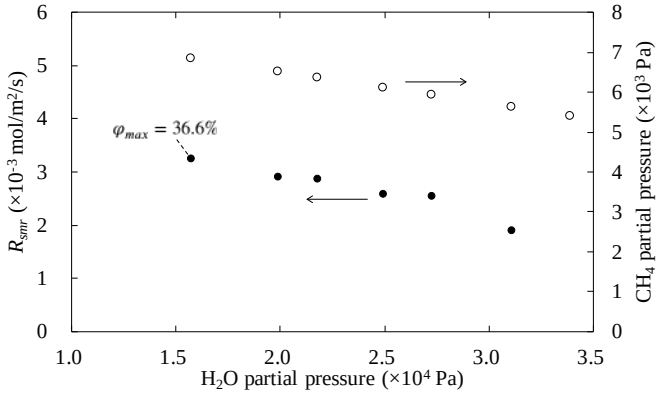

Figure 6. Dependence on steam partial pressure (condition Nos. 2,3,4,5,6,7).

During the experiments, the pressure at the inlet and outlet varied from 1.01×10^5 to 1.03×10^5 Pa because of fluctuations of the water surface level in the cold trap. The minimum methane conversion rate was 8.3% in test No.1. The maximum methane conversion rate was 36.6% in test No.2 and the thermocouple near the sample had a reading of 4.3℃ lower than that of the thermocouple installed in the furnace owing to the endothermic reaction. Figure 5 shows that R_{smr} monotonically increases with an increase of $P_{\mathrm{CH_4}}$, while a decreasing tendency is observed in figure 6 with an increase of $P_{\mathrm{H_2O}}$.

3.2.1. Coefficients a and b. From the above results and equations (9) and (10), contours of σ^{ab} is obtained as shown in figure 7. In this study, $a = 1.29$ and $b =$ -0.53 are selected to minimize σ^{ab}.

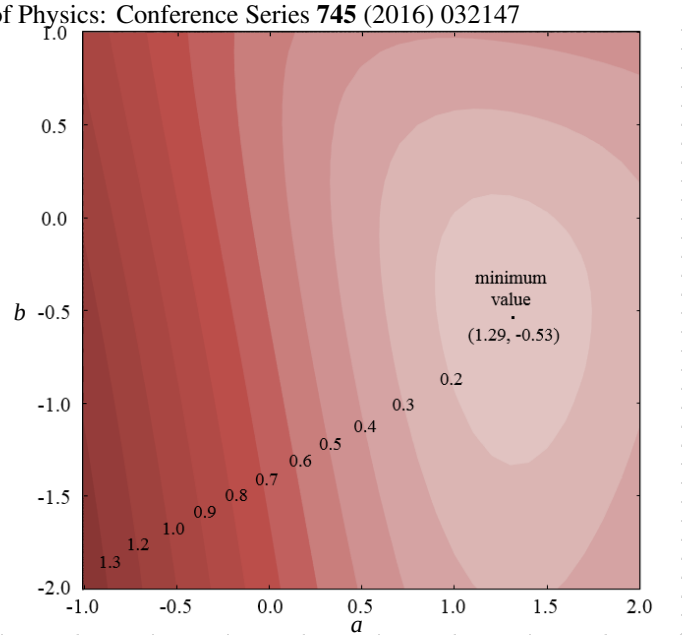

Figure 7. Contours of σ^{ab}.

3.2.2. Frequency factor and activation energy. The results of test No.7 and Nos.12 to 15 to investigate the temperature dependence are shown in figure 8 in the form of an Arrhenius plot. The maximum methane conversion rate was 30.5% in test No.12. Using equation (11), the frequency factor and activation energy are also calculated to be 1.42×10^3 (mol/m^2/Pa^{a+b}/s) and 1.56×10^5(J/mol), respectively by data fitting.

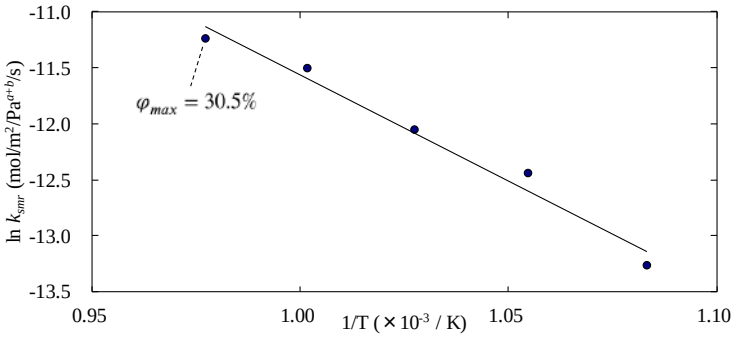

Figure 8. Arrhenius plot (condition Nos. 7,12,13,14,15).

Finally, the rate equation is obtained as

$$R_{smr} = 1.42\times10^3 \cdot \exp(-1.56\times10^5/\mathrm{R_0}T)\left(P_{\mathrm{CH_4}}\right)^{1.29}\left(P_{\mathrm{H_2O}}\right)^{-0.53} \quad (\mathrm{mol\,/\,m^2\,/\,s}) \qquad (12)$$

The activation energy and coefficients *a* and *b* in this study and previous studies are compared in table 4. The activation energy and coefficient *a* obtained in this study can be regarded as reasonable because they are in the range of previously reported values. Coefficient *b* in this study shows a negative dependence on the steam partial pressure similarly to in some previous studies [2] [11] [12] [14].

Table 4. Kinetic data reported for steam-methane reforming on Ni-YSZ.

Researchers	E (J /mol)	*a*	*b*	T (℃)
Lee *et al.* [2]	74000 - 98000	1.00	-1.25	800 - 1000
Ahmed and Forger [11]	95000	0.85	-0.35	850 - 900
Yakabe *et al.* [12]	191000	1.30	-1.20	-
Sciazko *et al.* [14]	117000	0.97	-0.08	550 - 750
King *et al.* [5]	11300 - 12400	1.00	0.00	650 - 800
Odegard *et al.* [13]	58000	1.20	0.00	900-1000
This study	156000	1.29	-0.53	650 - 750

3.3. Validity with different microstructures

To validate the equation (12), we conducted additional experiments using two extra samples having different microstructures. Reforming experiments and microstructure quantifications were conducted for the two samples. The main difference between the two samples is the Ni/YSZ volume ratio as shown in table 5.

Table 5. Microstructure properties.

	volume fraction				$S_{Ni\text{-}pore}$
	Ni	YSZ	Pore	Ni / YSZ ratio	(m^2/m^3)
sample A	0.132	0.524	0.344	0.252	151000
sample B	0.227	0.417	0.355	0.545	279000

The R_{smr} predicted by equation (12) are compared with the results of experiments in figures 9 and 10. The predicted R_{smr} generally agree with the experimental results when the methane partial pressure and/or temperature are relatively low. Differences between equation (12) and experiments gradually become larger with increase of the methane partial pressure or temperature. Furthermore, if we compare the experimental results of the two samples, the discrepancies from equation (12) are larger for the sample with a larger $S_{Ni-pore}$. These inconsistencies are the signs of non-uniform reaction inside the samples. Due to the large $S_{Ni-pore}$, the methane conversion rate is high particularly when the methane partial pressure or temperature is high. Combined with the relatively small porosity of the samples, the supply of the reactant gases to the inner part of the porous sample are limited. It lowers the local reaction rates in the samples. Because the reaction rates in the figures are the value averaged over the entire Ni surface area exposed to pore, the discrepancy from equation (12) becomes large when the methane conversion rate is high. The accuracy and reliability of the prediction can be improved by applying the local gas compositions and local temperature to equation (12). It is, however, difficult to obtain the local values experimentally. One can take the best advantage of the equation (12) if it is combined with a detailed numerical simulation that resolves the local gas compositions and temperature.

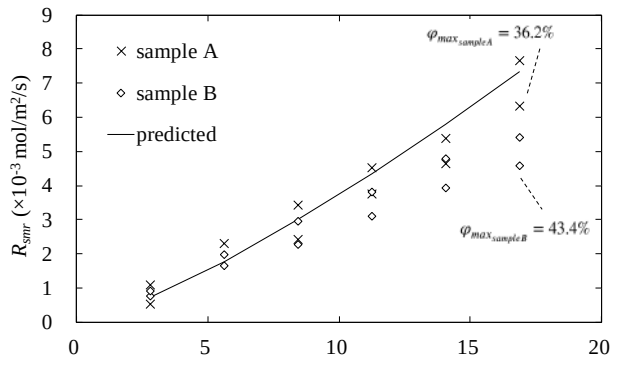

Figure 9. Dependence on the methane partial pressure.

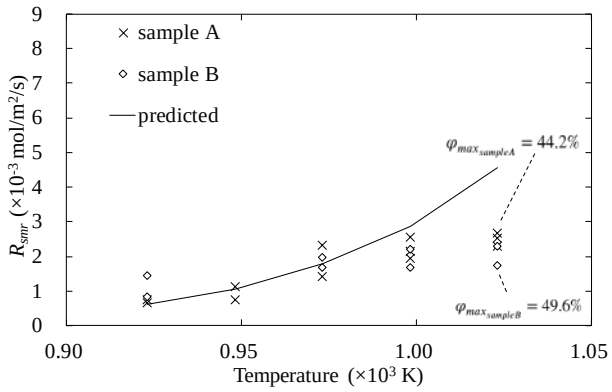

Figure 10. Dependence on temperature.

4. Conclusion

A rate equation for steam-methane reforming based on the Ni-YSZ anode microstructure was investigated in combination with an FIB-SEM technique. The kinetics described by a power-law expression showed a strong positive dependence on the methane partial pressure and negative dependence on the steam partial pressure. The obtained rate equation successfully reproduced the experimental results for Ni-YSZ samples having different microstructures in case of small methane consumption. This indicates that the methodology applied in this study is effective and practical.

References

[1] Iwai H, Yamamoto Y, Saito M and Yoshida H 2011 *Energy* **36** 2225-2234
[2] Lee A, Zabransky R and Huber W 1990 *Eng. Chem. Res.* **29** 766-773
[3] Achenbach E and Riensche E 1994 *J. Power Sources* **52** 283-288
[4] Mogensen D, Grunwaldt J-D, Hendriksen P V, Dam-Johansen K and Nielsen J U 2011 *J. Power Sources* **196** 25-38
[5] King D L, Strohm J J, Wang X, Roh H-S, Wang C, Chin Y-H, Wang Y, Lin Y, Rozmiarek R and Singh P 2008 *J. Catal.* **258** 356-365
[6] Bebelis S, Zeritis A, Tiropani C and Neophytides S G 2000 *Eng. Chem. Res.* **29** 4920-4927
[7] Boder M and Dittmeyer R 2006 *J. Power Sources* **155** 13-22
[8] Iwai H *et al.* 2010 *J. Power Sources* **195** 955-961
[9] Eguchi K, Kojo H, Takeguchi T, Kikuchi R and Sasaki K 2002 *Solid State Ionics* **152-153** 411-416
[10] Sangtongkitcharoen W, Assabumrungrat S, Pavarajarn V, Laosiripojana N and Paraserthdam P 2005 *J. Power Sources* **142** 75-80
[11] Ahmed K and Forger K 2000 *Catal. Today* **63** 479-487
[12] Yakabe H, Ogiwara T, Hishinuma M and Yasuda I 2001 *J. Power Sources* **102** 144-154
[13] Odegard R, Johnsen E and Karoliussen H 1995 *Proc. Fourth International Symposium on Solid Oxide Fuel Cells (SOFC-IV)* pp.810-819
[14] Sciazko A, Komatsu Y, Brus G, Kimijima S and Szmyd Janusz S. 2014 *Int. J. Hydrogen Energy* **39** 16372-16389